The impacts of climate change on tropical-to-extratropical transitions in the North-Atlantic basin

Aude Garin[1], Francesco S.R. Pausata[1], Mathieu Boudreault[1], Roberto Ingrosso[1]

[1]Department of Earth and Atmospheric Sciences, Université du Québec à Montréal, Montréal, Québec, Canada

Correspondence to: Aude Garin (garin.aude@courrier.uqam.ca)

Abstract. As tropical cyclones migrate towards mid-latitudes, they can transform into extratropical cyclones, a process known as extratropical transition. In the North Atlantic basin, nearly half of the hurricanes undergo this transition. After transitioning, these storms can reintensify, posing significant threats to populations and infrastructure along the eastern coast of North America. While the impacts of climate change on hurricanes have been extensively studied, there remain uncertainties about its effects on extratropical transitions. This study aims to assess how climate change affects the frequency, location, intensity, and duration of these transitions. To achieve this, high-resolution regional simulations from an atmospheric regional climate model, based on the RCP 8.5 emissions scenario, were used to compare two 30-year periods: the present (1990-2019) and the end of the century (2071-2100). The results indicate a projected decrease in the number of tropical hurricanes, with no significant change in extratropical transition rates. September and October continue to be the primary months for extratropical transitions. However, the season's peak appears to have shifted from September to October, suggesting that large-scale environmental conditions may become more favorable for extratropical transitions in October in the future. Although a poleward shift in the maximum intensity of tropical hurricanes is detected, the average latitude of the transitions does not change. Our findings suggest that transitioning storms will be more intense in the future, despite a less baroclinic atmosphere due to a stronger contribution from latent heat transfer. However, the risk of reintensification after transition is not expected to increase.

1. INTRODUCTION

Tropical cyclones can transform into extratropical cyclones through a process called extratropical transition (ET), in particular when they encounter a baroclinic environment and experience cooler sea surface temperatures. These transitions occur rather frequently in the North Atlantic basin, with approximately 50% of hurricanes having undergone an ET over the period 1950-2001 (Hart & Evans, 2001). Moreover, about 50% of tropical cyclones that made landfall during this period were in the process of transitioning (Hart & Evans, 2001). Some of these cyclones can intensify after transitioning, resulting in significant harm to human lives and damage to infrastructures, as seen with Hurricane Floyd (1999) and Hurricane Sandy (2012). More recently, Hurricane Fiona in 2023 has set a new record for the lowest pressure ever recorded in Canada (Chedabucto Bay). The North-Eastern Coast of the United States and the Canadian Maritimes, which typically experience 1-2 of these storms per year, as well as Western Europe, which faces them once every two years, are particularly vulnerable to these risks (Hart & Evans, 2001). Given the substantial financial losses these events can cause, there are growing concerns among economic stakeholders about the potential impact of climate change on the frequency and severity of these transitions.

The atmospheric mechanisms underlying extratropical transitions have been extensively studied in recent years. As a tropical cyclone moves poleward, it encounters several environmental changes, such as low sea surface temperature (SST), increased SST gradients, enhanced vertical wind shear, and a stronger Coriolis force (Jones et al., 2003). These changes may remarkably affect the tropical cyclone, resulting in a loss of

44   intensity, a breakdown of its warm-core structure, and a loss of its axisymmetric structure (Jones et al., 2003).
45   When a tropical cyclone encounters an existing extratropical system, typically a mid-tropospheric trough,
46   the process of extratropical transition may be initiated (Hart et al., 2006; Jones et al., 2003; Klein et al., 2000).
47   The mid-tropospheric trough favors the advection of the angular momentum – rather than the heat advection
48   – which drives the conversion of the cyclone's warm-core structure into a cold-core structure (Hart et al.,
49   2006). This advection of angular momentum disturbs the classic structure of a tropical cyclone, characterized
50   by a decrease in wind strength with height and a warm core, thereby disturbing the thermal wind balance. To
51   restore thermal wind balance, a secondary circulation is established: above the maximum of angular
52   momentum advection, adiabatic descent causes warming, while below the maximum, adiabatic ascent leads
53   to cooling, resulting in frontogenesis (Harr & Elsberry, 2000; Hart et al., 2006). During this transition, the
54   storm's wind field expands and becomes asymmetric, shifting the location of maximum wind speeds (Evans
55   & Hart, 2008).

56   Hence, the mid-latitude environment and weather systems play an essential role in a tropical cyclone's
57   transition process. During and after the extratropical transition, the addition of baroclinic energy (Evans et
58   al., 2017) and diabatic heating (Rantanen et al., 2020) may cause an intensification of post-transition tropical
59   cyclones.

60   While the impact of climate change on tropical cyclones has been largely addressed in recent years, only a
61   few studies have focused on the effects of a warmer climate on extratropical transition events. Regarding
62   tropical cyclones, it is expected that their global frequency may decrease in a warmer environment, although
63   the proportion of very intense hurricanes (especially Category 4 and 5 events) is likely to increase (Bender
64   et al., 2010; Hill & Lackmann, 2011; Knutson et al., 2020; Mallard et al., 2013). Additionally, there may be
65   a poleward expansion of tropical cyclone genesis (Garner et al., 2021) along with a poleward migration of
66   the maximum intensity of tropical cyclones (Lee et al., 2020) due to higher SSTs and reduced wind shear at
67   mid-latitudes. However, there remain uncertainties around this latter point (Knutson et al., 2020). In the mid-
68   latitude environment, a decrease in vertical wind shear (Kossin et al., 2014) and a reduction in the frequency
69   of extratropical systems during the summer season in the Northern Hemisphere (Lehmann et al., 2014) are
70   anticipated. Consequently, storms might become more intense during extratropical transition due to the
71   projected increase in the intensity of tropical cyclones. Furthermore, extratropical transitions may occur
72   farther north. Warmer SSTs could enable tropical cyclones to maintain their tropical characteristics and
73   strength further north, thereby increasing the likelihood of encountering a baroclinic zone necessary for
74   extratropical transition (Hart & Evans, 2001). However, the potential projected decrease in extratropical
75   systems during summer (Lehmann et al., 2014), along with the reduction in baroclinicity in the low
76   troposphere, may hinder extratropical transitions.

77   Regarding extratropical transitions in a warmer environment, they are expected to be more intense, last
78   longer, and be associated with heavier precipitation (Jung & Lackmann, 2019, 2021, 2023; Michaelis &
79   Lackmann, 2019, 2021). However, post-transition storms are expected to be less intense (Jung & Lackmann,
80   2021, 2023). An increase in the frequency of extratropical transition events is anticipated in the central and
81   eastern North Atlantic basin (Baker et al., 2022; Liu et al., 2017), consistent with the projected poleward and
82   eastward expansion of tropical cyclone genesis regions. However, there is still uncertainty about how
83   extratropical transition events will evolve in a warmer environment.

84   Our study aims to determine the impacts of climate change on the frequency, location, duration and intensity
85   of extratropical transitions in the North Atlantic basin by using high-resolution simulations from a regional
86   atmospheric climate model that span two 30-year periods: 1990-2019 for present-day simulations and 2071-
87   2100 for simulations of the future. Simulations of future climate are based on the Representative
88   Concentration Pathways 8.5 (RCP 8.5) scenario. The focus of the study is particularly on highly populated
89   areas (U.S. Northeastern Coast and Canadian Maritimes) where casualties and infrastructure damages can be
90   significant.

91   This paper is organized as follows: Section 2 describes the data and methodology used to track tropical
92   cyclones and extratropical transition events, as well as the key metrics used to assess the change in

93   extratropical transitions (ET). Section 3 presents the key findings on how climate change impacts the
94   frequency, location, and intensity of ET. .Section 4 discusses these findings and provide conclusions.

95   **2.   EXPERIMENTS AND METHODS**

96   **2.1   Data experiments and model description**
97   The two 30-year experiments used for this study are part of the set of simulations used in Ingrosso & Pausata
98   (2024). These experiments encompass the present-day scenario (1990-2019) and the RCP 8.5 future scenario
99   (2071-2100). We chose to focus on the most extreme scenario to determine whether any significant impacts
100 emerge, as scenarios with lower greenhouse gas emissions are less likely to produce a discernible signal.

101 These experiments were performed with the developmental version of the Canadian Regional Climate
102 Model/Global Environmental Multiscale (CRCM5/GEM 4.8) at a horizontal grid spacing of 0.12° and 57
103 vertical levels. The regional model CRCM5 was driven using the data from the global simulations performed
104 with GEM4.8 at 0.55° horizontal resolution and 73 vertical levels (further details can be found in Ingrosso &
105 Pausata (2024)).

106 To evaluate the model's performance, the regional model was compared with observations from the Tropical
107 Rainfall Measuring Mission (TRMM), the Climate Research Unit, and one reanalysis product (ERA5),
108 focusing on the mean precipitation distribution from 2000 to 2019. The regional model demonstrated its
109 ability to align with the observations despite a persistent dry bias in the median and lower percentiles.
110 Additionally, the regional model has shown good performance in reproducing the general diurnal cycle,
111 although rainfall was underestimated compared to satellite observations.

112 The regional area covered by the simulations extends from 3°S to 48°N and from 81°W to 52°E.

113 **2.2   Storm Tracking algorithm**
114 In this study, we employ a storm-tracking algorithm designed to detect both tropical cyclones (including
115 tropical storms) and transitioning tropical cyclones. This algorithm is based on the methodology used in
116 Dandoy et al. (2021) and follows a three-step procedure: storm identification, storm tracking, and storm
117 lifetime, in line with previous studies (Gualdi et al., 2008; Scoccimarro et al., 2017). The algorithm uses 3-
118 hour outputs of the model for the period from June to December.

119 *Storm identification*
120 A storm is identified when several criteria are met. One of the key strengths of this algorithm is the double-
121 filtering approach that prevents from double-counting a tropical cyclone (TC) when there is a temporary
122 decrease in intensity, followed by a restrengthening. Specifically, each storm center is categorized as either
123 a weak center (if it meets only loose criteria) or as a strong center (if it also meets strict criteria). The criteria
124 used are as follows:

125 -   Surface pressure: The center's surface pressure must be lower than 1013 hPa (1005 hPa to be
126   classified as a strong center) and represent a minimum within a 250 km radius. Additionally, the
127   center must be a closed low-pressure system, with the minimum pressure difference between the
128   center and a circle of grid points in small (400 km) and large (800 km) radii around the center
129   exceeding 1 and 2 hPa, respectively (4 and 6 hPa to be considered as a strong center).
130 -   850-hPa vorticity: The maximum 850-hPa vorticity within a 200-km radius around the center must
131   exceed 10^{-5} s^{-1} (10^{-4} s^{-1} to be considered as a strong center).
132 -   10m wind: The maximum wind speed at 10 meters within a 100-km radius around the center must
133   exceed 8 m/s (17.5 m/s to be considered as a strong center).

134 In this study, the criterion based on temperature anomalies was not used to reject centers, thus allowing for
135 the detection of warm-core storms such as transitioning tropical storms. However, the algorithm still applies

136 a strict criterion for identifying strong centers. Specifically, this criterion requires that the sum of the
137 temperature anomalies at 250, 500 and 700 hPa, defined as the difference between the maximum temperature
138 and the mean temperature within a 200 km radius around the center, must exceed 2°C.

139 *Storm tracking*
140 The purpose of this step is to assign each identified center to an existing storm or, if no existing storm can be
141 linked to the detected center, to consider it as the origin of a new storm. Initially, centers that are more than
142 250 km apart are treated separately. If two centers are within this distance, only the center with the strongest
143 vorticity is retained. Storms are tracked using the nearest-neighbor method, a technique also employed in
144 various studies (Blender et al., 1997; Blender & Schubert, 2000; Schubert et al., 1998). For each existing
145 storm, the algorithm predicts the potential location of the next center based on the historical trajectory of the
146 previous two centers. A new center is then assigned to the storm whose predicted location is closest, with
147 preference given to the nearest center.

148 *Storm lifetime*
149 For each determined track, the following final conditions must be met:

150 - The lifetime of the storm must exceed 36 hours.
151 - The storm must have at least 12 strong centers.
152 - The minimum travel distance must be at least 10° of combined latitude and longitude.
153 - The number of strong centers must account for at least 77% of the core trajectory, which is defined
154   as the path between the first and the last strong center.

155 **2.3 Detection of extratropical transitions (ET)**
156 The removal of the warm-core loose criterion enables the algorithm to detect both warm-core and cold-core
157 centers. Simultaneously, the use of the warm-core strict criterion ensures that only storms that have
158 experienced a tropical cyclone phase are detected.

159 ET events are identified using the Cyclone Phase Space (CPS) methodology developed by Hart (2003) and
160 widely employed in previous studies focusing on ET (Baker et al., 2022; Hart et al., 2006; Jung & Lackmann,
161 2019, 2021, 2023; Liu et al., 2017). This methodology involves three parameters: the lower-tropospheric
162 thermal axisymmetry of the cyclone (B), the lower-tropospheric ($-V_T^L$) and the upper-tropospheric ($-V_T^U$)
163 thermal winds. These three parameters describe and differentiate the structure of tropical cyclones,
164 characterized by a warm-core and vertically stacked structure, from that of extratropical cyclones,
165 characterized by a cold-core and tilted structure.

166 The use of high-resolution data ensures reliable CPS diagnostics (Hart, 2003).

167 *Cyclone thermal symmetry (B)*
168 This parameter allows for identifying the frontal nature of the cyclone, or the absence thereof. It is defined
169 as the storm-motion-relative 900-600 hPa thickness asymmetry within a 500-km radius (Hart, 2003). For the
170 Northern Hemisphere, B is defined as:

$$B = \left(\overline{Z_{600\,hPa} - Z_{900\,hPa}}\big|_R - \overline{Z_{600\,hPa} - Z_{900\,hPa}}\big|_L \right) \tag{1}$$

171 where Z represents the geopotential height, R and L indicate the right and left sides of storm motions, and the
172 overbar denotes the mean area over a semicircle with a radius of 500 km.

173 Very low values of B are associated with non-frontal storms such as TCs, while high values of B are
174 associated with frontal storms such as extratropical cyclones. Hart (2003) suggests that a threshold of 10m is
175 appropriate for distinguishing non-frontal storms from frontal storms. This threshold has been widely utilized
176 in other studies focusing on ET (Baker et al., 2022; Hart et al., 2006; Jung & Lackmann, 2019, 2021, 2023;

177 Liu et al., 2017). However, Zarzycki et al. (2017) indicate that a threshold of 15 m is more appropriate
178 threshold when using high-resolution.

179 To calculate the average speed of the 900-600 hPa layer, we considered four sub-layers: 900-850 hPa, 850-
180 800 hPa, 800-700 hPa, and 700-600 hPa. The mean zonal and meridional speeds for each layer were
181 computed as follows:

$$\bar{u_i} = \sum_{j \in D} u_{i,j} \tag{2}$$

182 where D represents the 500km-radius circle around the center.

183 Then, the total mean zonal and meridional speeds are defined as the weighted average of the mean speeds
184 calculated for each sub-layer:

185

$$\bar{u} = \sum_{i=1,4} \bar{u_i}\omega_i \tag{3}$$

186 where ω_i represents the weight of the layer i.

187 The left layer comprises the points that satisfy the following criteria:

$$\frac{\pi}{180}R(lat_{i,j} - lat_{i_0,j_0}) > \frac{\pi}{180}R\frac{\bar{v}}{\bar{u}}cos\left(\frac{\pi}{180}lat_{i,j}\right) \tag{4}$$

188 and the thickness of the layer is thus defined as:

$$thickness = \frac{1}{N_L}\left(\sum_{k=1}^{N_L} GZ_{600,k} - GZ_{900,k}\right) \tag{5}$$

189 where N_L is the number of points within the layer.

190 The same methodology is also applied to the right layer, which is defined as:

$$\frac{\pi}{180}R(lat_{i,j} - lat_{i_0,j_0}) < \frac{\pi}{180}R\frac{\bar{v}}{\bar{u}}cos\left(\frac{\pi}{180}lat_{i,j}\right) \tag{6}$$

191

192 *Lower and upper thermal winds*
193 Tropical cyclones are characterized by a decrease in height perturbation with increasing altitude. In contrast,
194 for extratropical cyclones, the height perturbation decreases with height.

195 In this study, the height perturbation ΔZ is calculated as the difference between the maximum geopotential
196 height and the minimum geopotential height within a 500 km-radius circle ($\Delta Z = Z_{max} - Z_{min}$) and is
197 proportional to the magnitude of the geostrophic wind (V_g)(Hart, 2003)

198

$$\Delta Z = \frac{dg|V_g|}{f} \tag{7}$$

5

199 where d represents the distance between the two geopotential extrema, f is the Coriolis parameter, and g is
200 the gravity constant.

201 Scaled thermal winds can be defined as (Hart, 2003):

$$-V_T^L = \left.\frac{\partial \Delta Z}{\partial ln(p)}\right|_{900\ hPa}^{600\ hPa} \tag{8}$$

202 and

$$-V_T^U = \left.\frac{\partial \Delta Z}{\partial ln(p)}\right|_{600\ hPa}^{300\ hPa} \tag{9}$$

203 A positive value of $-V_T^L$ (*ie* $-V_T^U > 0$) indicates a warm-core structure in the lower (*ie* upper) troposphere,
204 while a negative value of $-V_T^L$ (i.e. $-V_T^U < 0$) indicates a cold-core structure in the lower (i.e. upper)
205 troposphere. During ET, the signs of $-V_T^L$ and $-V_T^U$ may differ.

206 As recommended by Hart (2003), we conducted a linear regression on the vertical profile of ΔZ to estimate
207 the thermal wind parameters. The levels used for these regressions are: 900 hPa, 850 hPa, 800 hPa, 700 hPa,
208 600 hPa, 500 hPa, 400 hPa, and 300 hPa.

209 *Detection of ET events* To mitigate the variability in parameters caused by numerical noise, a 12-hour
210 smoothing window is applied, following the recommendations of Michaelis & Lackmann (2019), who
211 employed a 24-hour smoothing window. Additionally, a filtering algorithm was employed to exclude highly
212 chaotic trajectories characterized by multiple transitions. The core principles of this algorithm are:

213   - Exclusion of ET events occurring below 20° as ET events rarely occur below this threshold (Hart &
214   Evans, 2001)
215   - When multiple transitions occur, only the final transition is considered, provided that no reverse
216   transition follows it.

217 For this study, the onset of ET is detected when (Liu et al., 2017; Michaelis & Lackmann, 2019):

218   - $\tilde{B} > 15\ m$ or $-\widetilde{V_T^L} < 0$

219 And the completion of ET is detected when both criteria are simultaneously met.

220 In other studies (Hart, 2003; Hart et al., 2006; Jung & Lackmann, 2021), the onset of ET was detected when
221 B exceeded the threshold. However Liu et al. (2017) argued that this methodology might be inadequate for
222 capturing TCs that transition to cold-core systems before developing an asymmetric structure.

223 **2.4   The Eady Growth Rate: An Indicator of the baroclinicity**
224 The Eady Growth Rate (EGR) is a widely used indicator of the baroclinicity of the environment (Eady, 1949).
225 ET are more likely to occur in zones associated with high values of EGR. It is defined as follows (Lindzen
226 & Farrell, 1980):

$$\sigma = 0.31 \frac{|f|}{N}\left|\frac{dV}{dz}\right| \tag{10}$$

227 where f is the Coriolis parameter, $\frac{dV}{dz}$ is the vertical wind shear, and N is the Brunt-Väisälä frequency:

$$N = \sqrt{\frac{g}{\theta}\frac{\partial \theta}{\partial z}} \tag{11}$$

228   where θ is the virtual potential temperature, and g is the gravity constant

229   In this study, we mainly focused on mid-troposphere baroclinicity and, therefore, computed the EGR at 500
230   hPa using the geopotential heights, humidity, meridional and zonal wind speeds, and temperatures at 400 hPa
231   and 500 hPa.

2.5   Integrated Kinetic Energy: An indicator of the storm intensity

232

233   The concept of Integrated Kinetic Energy (IKE) was first introduced by Powell & Reinhold (2007), who
234   demonstrated that this indicator might better assess a hurricane's destructive potential than the maximum
235   sustained surface wind speed, as it accounts for storm size.

236   IKE is the integration of the 10-m kinetic energy per unit volume over a domain volume (V) centered around
237   the storm's center. IKE is given by:

$$IKE = \int_V \frac{1}{2} \rho U^2 dV \qquad (12)$$

238   where ρ is the air density and U is the 10-m wind velocity.

239   Assuming an air density value of 1 kg/m^3 and a volume height of 1m, the expression can be simplified as
240   follows (Cheung & Chu, 2023):

$$IKE = \int_A \frac{1}{2} U^2 dA \qquad (13)$$

241   In this study, the area considered is a circle with a 500km radius, centered around the TC center.

2.6   Minimal theoretical pressure of a TC

242

243   The minimal theoretical pressure allows to estimate the minimum pressure a TC center can reach, based on
244   the SST and the atmospheric profile ((Bister & Emanuel, 2002). This critical pressure p_c is given by the
245   following equation:

$$R_d T_s ln\left(\frac{p_a}{p_c}\right) = \frac{1}{2}\left(\frac{T_s}{T_0}\frac{C_k}{C_D}(CAPE^* - CAPE_{env})|_{RMW}\right) + CAPE_{env}|_{RMW} \qquad (14)$$

246   where p_a is the environmental pressure, T_s is the SST, T_0 is the outflow layer temperature, C_k and C_D are
247   the enthalpy and momentum surface exchange coefficient, and R_d is the ideal gas constant for dry air.
248     $CAPE^*|_{RMW}$ is the Convective Available Potential energy of a saturated air parcel and $CAPE_{env}|_{RMW}$ is the
249   environmental Convective Available Potential Energy.

250   The minimum theoretical pressure was calculated with the pyPI package from Python (Gilford, 2021).

2.7   Statistical analysis

251

252   For the statistical assessment of the differences, the Mann-Whitney-Wilcoxon test was used to compare the
253   distributions. This test is recommended when the normality assumption cannot be made.

254   A significance level of 10% was considered.

2.8   Validation

255

256   The annual ET ratio, defined as the ratio of the yearly number of ET events to the yearly number of tropical
257   cyclones, was computed for the 1990-2019 period of the present-day experiment. This frequency was then

258   compared with observational data from the International Best Track Archive for Climate Stewardship
259   (IBTRACS, Knapp et al., 2010) and with reanalysis data ECMWF reanalysis (ERA5, Hersbach et al., 2020),
260   to which the tracking algorithm was applied within the same spatial domain as the present-day experiment.

261   The results demonstrate the current experiment's strong ability to reproduce the mean annual ET ratio despite
262   exhibiting a lower distribution variability than ERA5 and IBTRACS (Fig. 1).
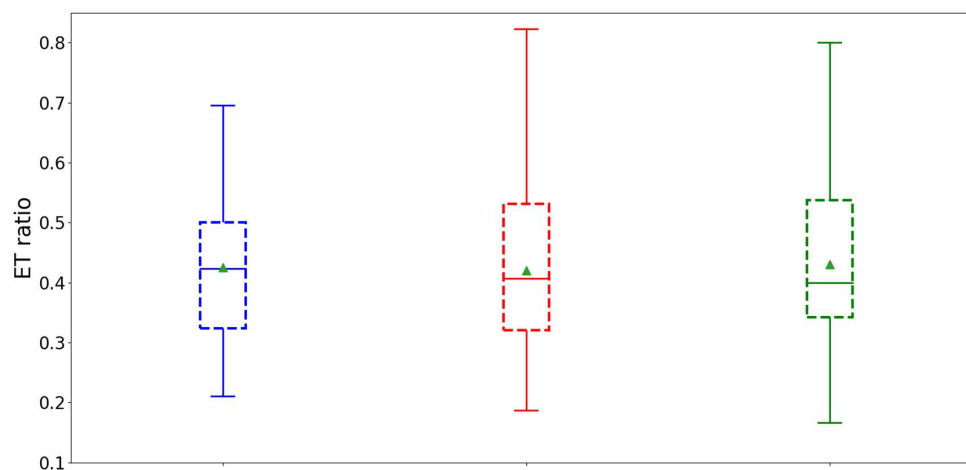
263

264   **Figure 1:** Box plot of the ET ratio for the present-day simulation (blue), ERA5 (red), and IBTRACS (green).
265   The box represents the interquartile range (IQR), containing 50% of the data; the upper edge of the box
266   represents the 75th percentile (upper quartile -UQ) while the lower edge is the 25th percentile (lower quartile
267   – LQ). The horizontal line within the box indicates the median, while the green triangle indicates the mean.
268   The whiskers extend to the smallest and largest data points within 1.5 times the IQR from the quartiles. Points
269   beyond the whiskers are considered outliers.

270

3. RESULTS

3.1   Tropical cyclones in present-day simulations and future climate simulations

The number of TCs, including tropical storms, is significantly lower (-3.7) in the future climate simulation (14.3) than in the present-day simulation (18). The season's peak remains in September for the future climate simulation (Fig. 2).
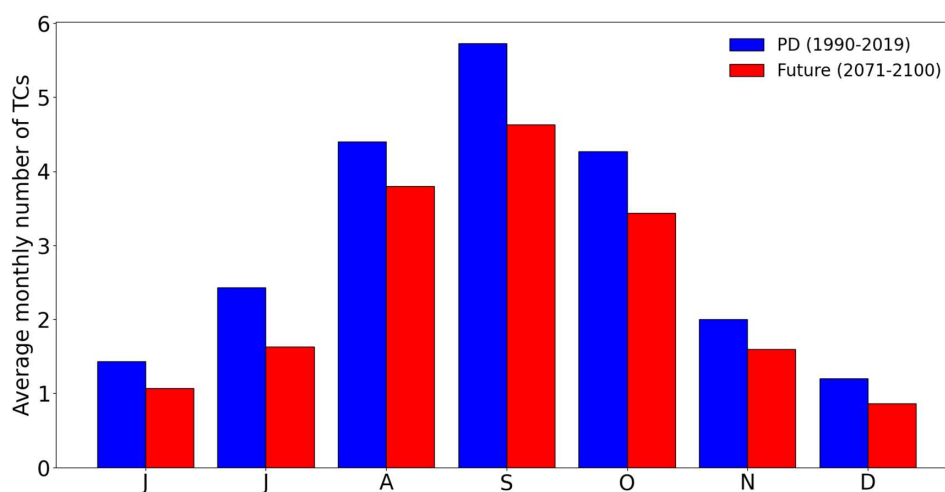

**Figure 2:** Average number of monthly TCs for the present-day (blue) and the future climate simulation (red) from June to December

For each tracked TC, the maximum intensity – defined here as the minimum pressure reached by the cyclone along its trajectory – was determined. Consistent with previous studies ((Hill & Lackmann, 2011; Knutson et al., 2020; Kossin et al., 2020), we found that there are more extreme events in the future climate simulation than in the present-day simulation (Fig. 3) and that the mean storm minimum pressure is deeper in the future climate simulation (-3 hPa).

Consistent with other studies (Lee et al., 2020; Studholme et al., 2022), the median TC maximum intensity is slightly shifted northwards of about 1.2° latitude (Fig. 4 a) in a warmer climate because of higher SST that help TCs sustain their intensity at higher latitudes.

9
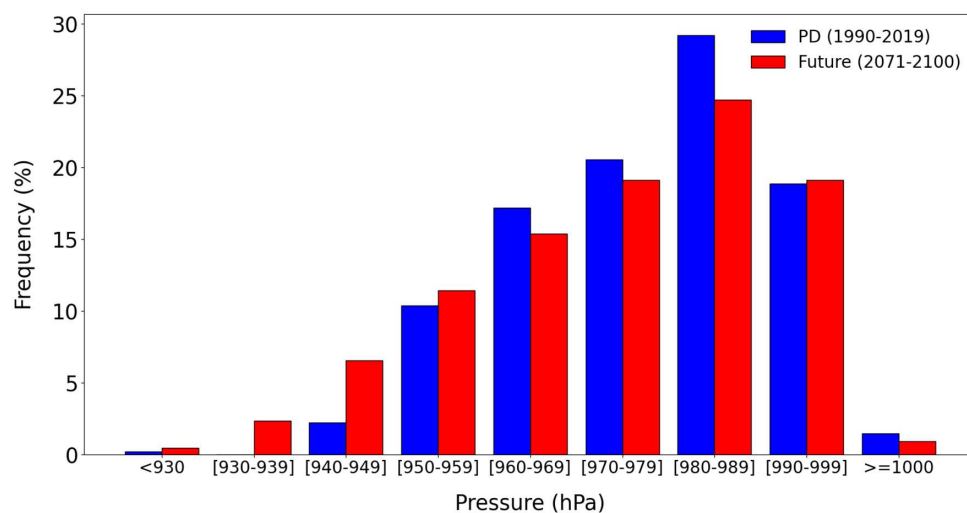
Figure 3: Distribution of the maximum intensity for the present-day (blue) and the future climate simulations (red). The maximum intensity is defined as the minimum pressure reached at the TC center during its lifetime.
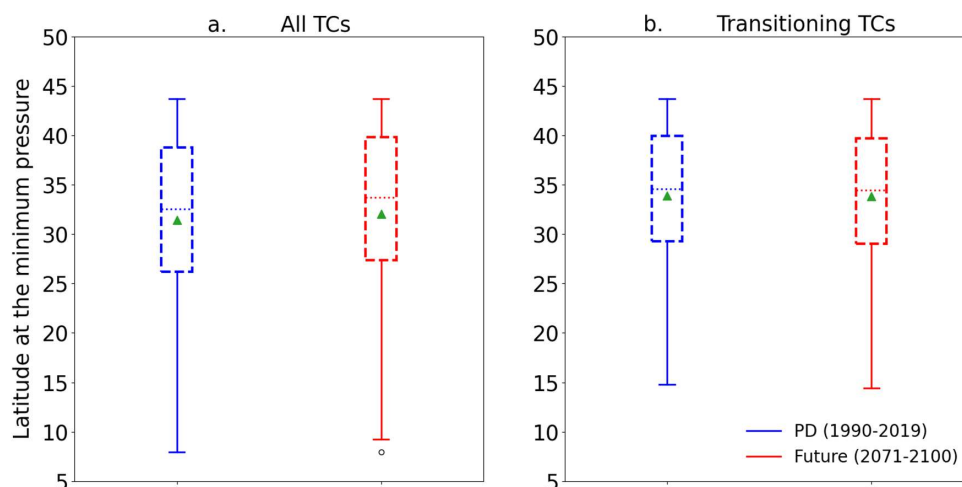
Figure 4: Box plot of the latitude of the minimum pressure for the present-day (blue) and the future climate (red) simulations a) for all TCs and b) for transitioning TCs. The box represents the interquartile range (IQR), containing 50% of the data; the upper edge of the box represents the 75th percentile (upper quartile- UQ) while the lower edge is the 25th percentile (lower quartile - LQ). The horizontal line within the box indicates the median, while the green triangle indicates the mean. The whiskers extend to the smallest and largest data points within 1.5 times the IQR from the quartiles. Points beyond the whiskers are considered outliers.

## 3.2 Change in the atmospheric baroclinicity

As expected, the mid-tropospheric available potential energy, represented by the Eady growth rate in the future climate simulation, is weaker than in the present-day simulation (Fig. 5a). This can be attributed to Arctic polar amplification, which reduces the thermal gradient between the high and tropical latitudes,

301 resulting in a weaker baroclinic zone. The difference is particularly pronounced at the mid-latitudes and on
302 the western side of the North Atlantic Ocean, where most transitions usually occur.

303 Conversely, the upper-tropospheric available potential energy is slightly higher in the future climate
304 simulation than the present-day simulation (Fig. 5b). That is consistent with the tropical upper-troposphere
305 warming effect, which increases the upper-tropospheric thermal gradient.
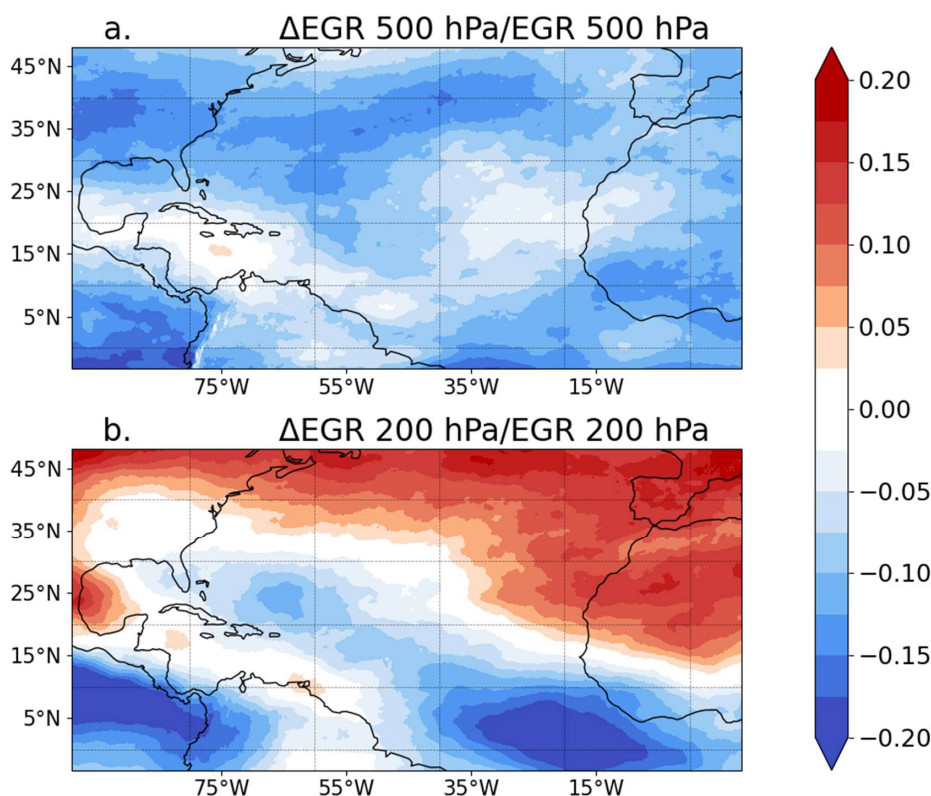
Figure 5: a) Relative difference in 500-hPa Eady Growth Rate between the future climate and the present-day simulations and b) Relative difference in 200-hPa Eady Growth Rate between the future climate and the present-day simulations

3.3 ET events and ET ratios

311 The mean annual number of ET events simulated in the future climate simulation (6.1) is significantly lower
312 than in the present-day simulation (7.6). The ET ratio, defined as the ratio of the number of ET events to the
313 number of TCs, is almost identical in the future climate simulation (42.7%) than in the present-day
314 simulations (42.6%).

315 Hart & Evans (2001) highlighted that ET events are more likely to occur if TCs maintain a minimum level
316 of intensity when they encounter a relatively strong baroclinic zone, enabling them to release the available
317 potential energy of the atmosphere. This minimum intensity level generally corresponds to a theoretical
318 minimum pressure of 960 hPa (Bister & Emanuel, 1998; Hart & Evans, 2001). Our findings indicate that the
319 northward shift of the baroclinic zone (Figure 7a) is balanced by a corresponding northward shift in the 960-
320 hPa theoretical minimum pressure (Figure 7b), thereby maintaining the relative position of this minimum

321   intensity level with respect to the favorable baroclinic regions. As a result, these factors may help to partially

322   explain why the probabilities of ET do not show significant differences.
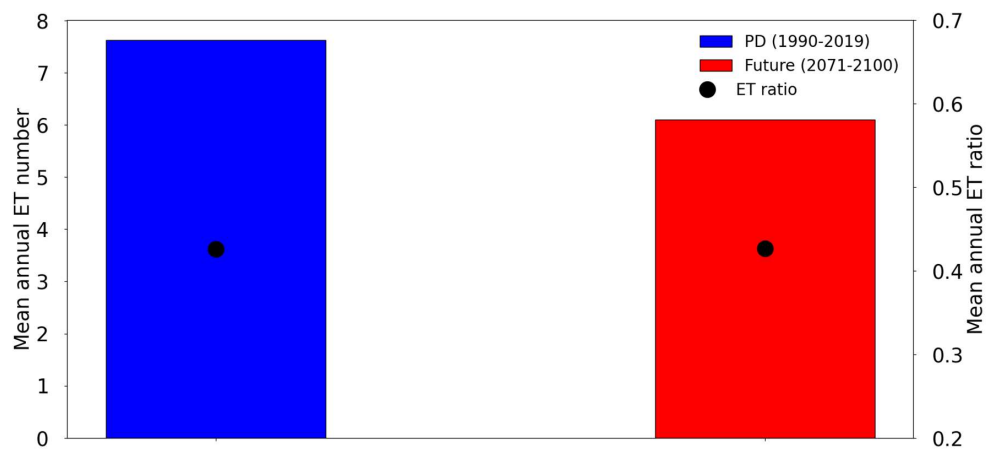
323

324   **Figure 6**: Mean annual ET numbers (bars, left axis) and mean annual ET ratio (dots, right axis) for the

325   present-day (blue) and the future climate (red) simulations. The ET ratio is defined as the ratio of number of

326   ET events to the number of TCs.

327
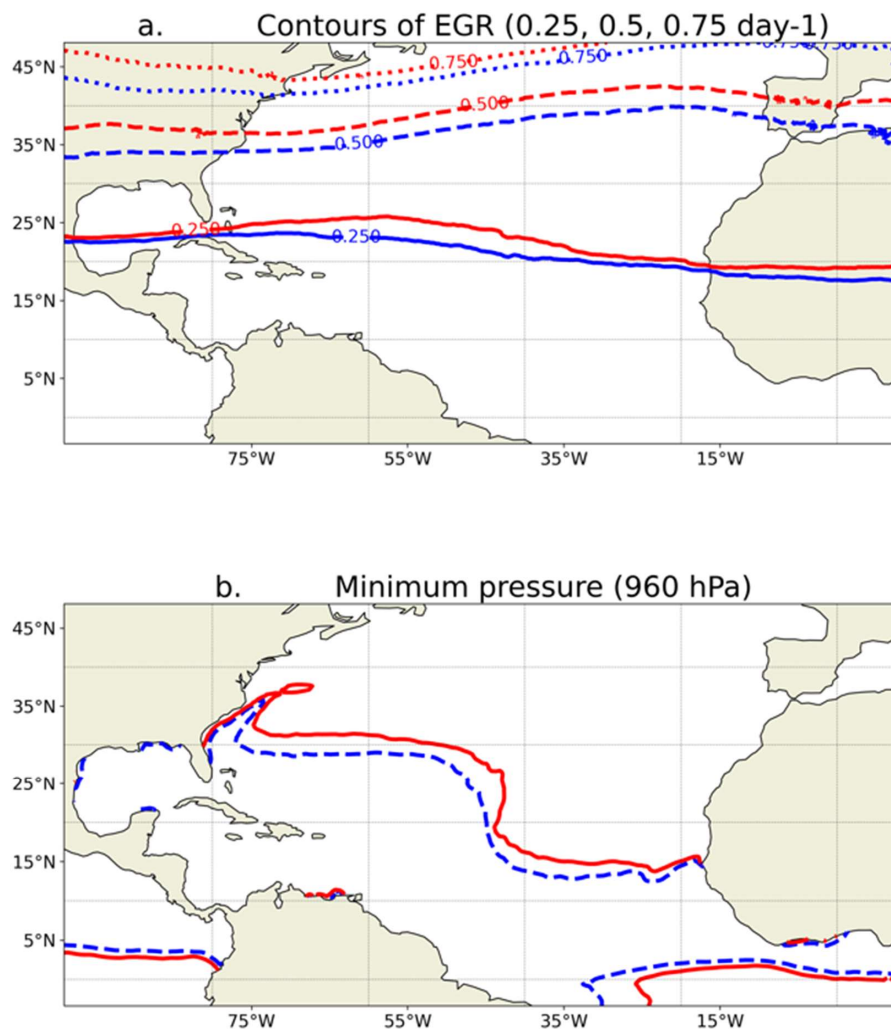
Figure 7: (a) Contours of mean Eady Growth rate for the present-day (blue) and the future climate (red) simulations. The solid lines represent the 0.25 day^{-1} level, the dashed lines represent the 0.5 day^{-1} level, and the dotted lines represent the 0.75 day^{-1} level. (b) Contours of the 960-hPa theoretical pressure for the present-day (blue dashed line) and the future climate (red solid line) simulations

3.4   ET seasonal cycle in future climate

To assess changes in the seasonality of ET events, the mean annual contribution of each month to the mean annual ET ratio was calculated. This indicator is calculated as follows: for each month and each year, the ET ratio is weighted by the monthly number of TC divided by the yearly total number of TC and then averaged over 30 years. This approach highlights the months when ET is most likely to occur, accounting for both the probability of TC occurrence and the conditional probability of ET.

In the present-day simulation, September and October are the most significant contributors to the annual ET ratio, as highlighted in Hart & Evans (2001). During these two months, the number of TCs and the baroclinic

340 energy remain relatively high, providing favorable conditions for ET events. In the future climate simulation,
341 September and October remain the months when the baroclinic energy levels are highest. However, the ET
342 season's peak appears to have shifted from September to October (Fig. 8). Indeed, in the future climate
343 experiment, the simulated decrease in October ET events mean number is less pronounced than the simulated
344 decrease in October mean number of TCs, suggesting a greater ET probability.
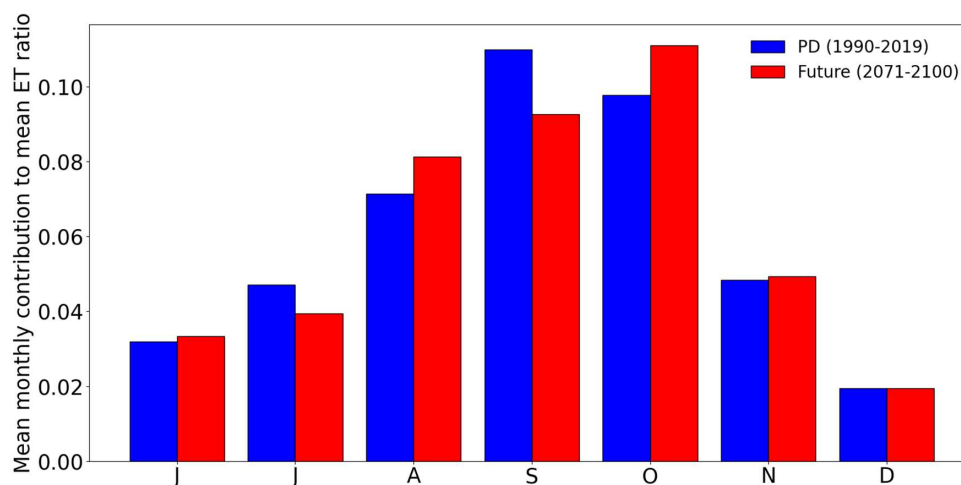
345

346 **Figure 8**: Monthly contribution to mean annual ET ratio for the present-day (blue) and the future climate
347 (red) simulations from June to December

348 **3.5   Location of ET onsets**
349 In this section, we focus on the impacts of ET locations, particularly to assess the threats they may pose to
350 the U.S. and Canada costal populations.

351 In both experiments, TCs that undergo ET reach their maximum intensity at higher latitudes compared to
352 those that do not undergo ET (Fig. 4 a and b). Indeed, TCs that are most likely to undergo ET need to sustain
353 a minimum energy level at middle latitudes. However, no significant northward shift in maximum intensity
354 location for TC undergoing ET is simulated (Fig. 4b). This finding partly explains why, despite the previously
355 highlighted northward shift in the baroclinic zone in future climate simulations (Figure 7a), transitions do not
356 occur further north (Fig. 9a) in the future climate simulation. These observations indicate that the mean
357 meridional displacement between the maximum intensity and the ET onset locations does not significantly
358 change under climate change. Additionally, the results show no significant change in the mean longitude of
359 ET onsets (Fig. 9 b).

360
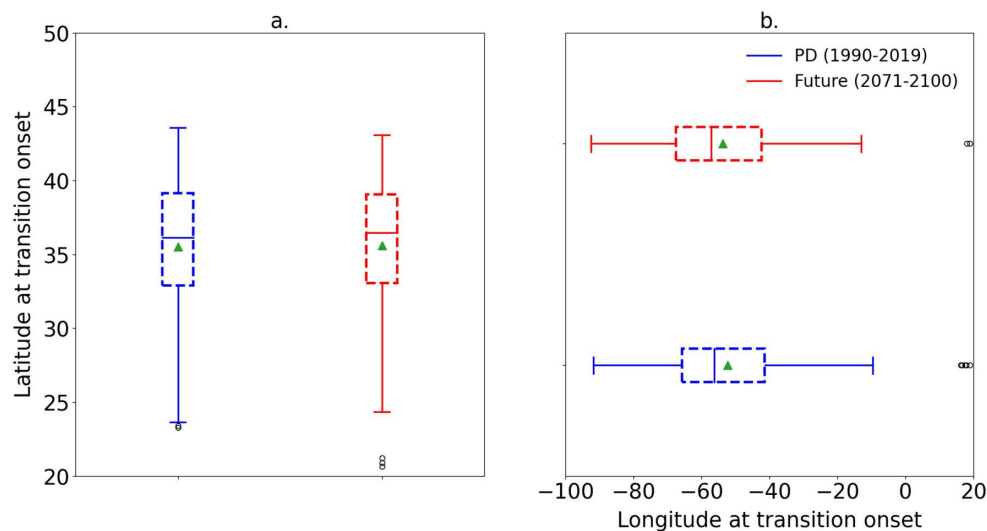
Figure 9: Box plot of the a) latitude of ET onset for the present-day (blue) and the future climate (red)
simulations and b) longitude of ET onset for the present-day (blue) and the future climate simulations (red).
The box represents the interquartile range (IQR), containing 50% of the data; the upper edge of the box
represents the 75th percentile (upper quartile - UQ) while the lower edge is the 25th percentile (lower quartile
- LQ). The horizontal line within the box indicates the median, while the green triangle indicates the mean.
The whiskers extend to the smallest and largest data points within 1.5 times the IQR from the quartiles. Points
beyond the whiskers are considered outliers.

The density map of ET onset, estimated with a Gaussian kernel, shows some differences (Fig. 10), with more
ET onsets occurring near the U.S. Northeastern coast around 35°N and 40 °N. This region corresponds to the
zone where a pronounced northward shift in the theoretical minimum pressure is simulated in the future
climate simulation compared to the present-day experiment (Fig. 7b).

372

373
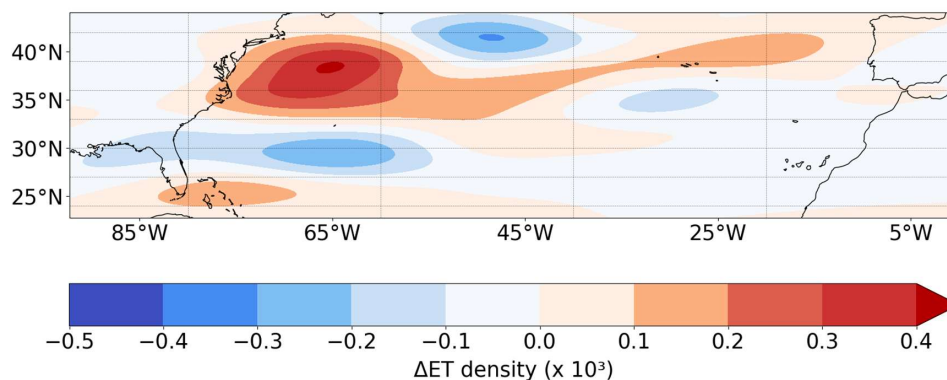
Figure 10: Difference in onset ET density between the future climate and the present-day simulations.

The overall lack of change in the mean ET onset latitude in the future climate simulation might be explained
by stronger tropical cyclones, which have slightly deeper low pressure (982 hPa compared to 986 hPa today)

15

377 at the time of ET onset, compensating for the weaker mid-tropospheric baroclinic zone that drives energy
378 release. Additionally, the upper-tropospheric baroclinic zone becomes stronger, further offsetting the mid-
379 tropospheric weakening. As a result, these factors balance out, preventing significant shifts in the average
380 latitude of extratropical transition onset.

381 **3.6   Duration of ET in Future Climate**
382 Here we investigate a potential change in the duration of ET events as high SSTs have been associated with
383 low-transitioning storms, which are generally stronger than fast-transitioning storms (Hart et al. ,2006). The
384 ET duration is defined as the time difference between the ET onset and ET completion. For ET events that
385 are not completed within the regional domain, the ET completion time is defined as the time when the storm
386 reaches the upper boundary of the spatial area.

387 The analysis shows no significant change in the ET duration for the future climate simulation compared to
388 the present-day experiment (Fig. 11 a). This conclusion also holds for storms where the transition is
389 completed within the regional domain (Fig. 11 b).
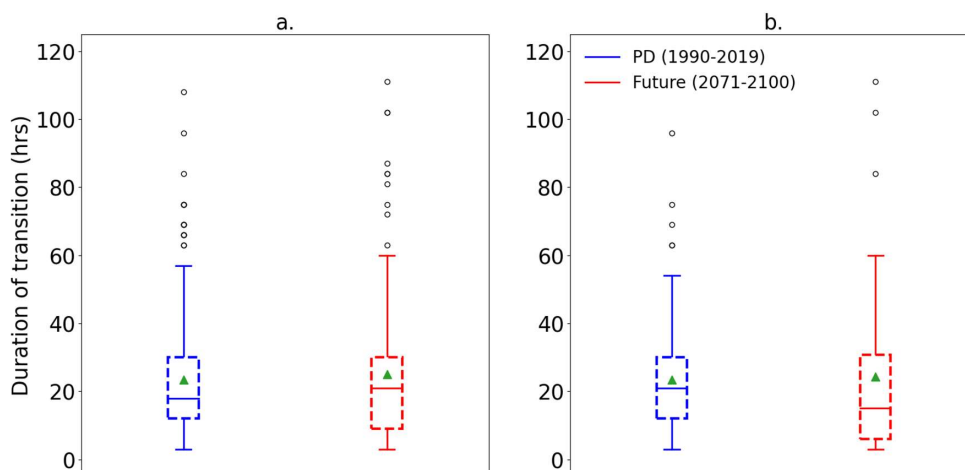
390

391 **Figure 11**: Box plot of the transition duration (in hours) for the present-day experiment (blue) and the future
392 climate simulations (red) for: a) all storms, and b) storms for which the transition is completed within the
393 regional zone. The box represents the interquartile range (IQR), containing 50% of the data; the upper edge
394 of the box is the 75th percentile (upper quartile - UQ) while the lower edge is the 25th percentile (lower quartile
395 - LQ). The horizontal line within the box indicates the median, while the green triangle indicates the mean.
396 The whiskers extend to the smallest and largest data points within 1.5 times the IQR from the quartiles. Points
397 beyond the whiskers are considered outliers.

398 **3.7   Energetics of Transitioning Storms in Future Climate**
399 This section explores the energetic changes in transitioning storms under future climate scenarios, focusing
400 on how their destructive potential evolves and the factors contributing to these changes. The destructive
401 potential of transitioning storms is notably higher (+20.5%) in the future climate simulation relative to present
402 day. This increase is reflected in the cumulative IKE over the transition period, which is significantly higher
403 in future climate simulations (Fig. 12). This increased destructive potential is partly attributed to a
404 significantly higher latent heat flux (+17%, Fig. 13 a) in the future climate simulation during the transition,
405 driven by higher SSTs. As expected, the available potential energy is significantly weaker in the future
406 climate simulation (Fig. 13 b), suggesting a reduction in baroclinic conversion.
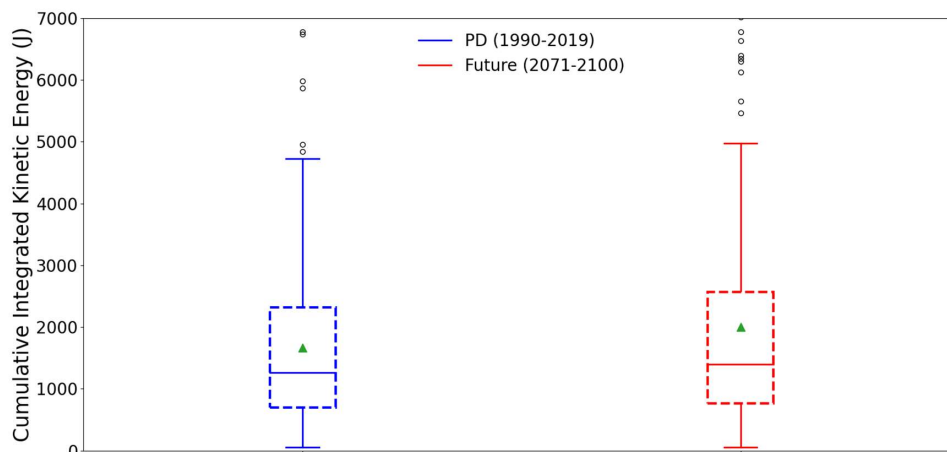
Figure 12: Box plot of Cumulative Integrated Kinetic Energy (in Joules) during the transition for the present-day experiment (left) and the future climate simulation (right). The box represents the interquartile range (IQR), containing 50% of the data; the upper edge of the box represents the 75th percentile (upper quartile - UQ) while the lower edge is the 25th percentile (lower quartile - LQ). The horizontal line within the box indicates the median, while the green triangle indicates the mean. The whiskers extend to the smallest and largest data points within 1.5 times the IQR from the quartiles. Points beyond the whiskers are considered outliers.
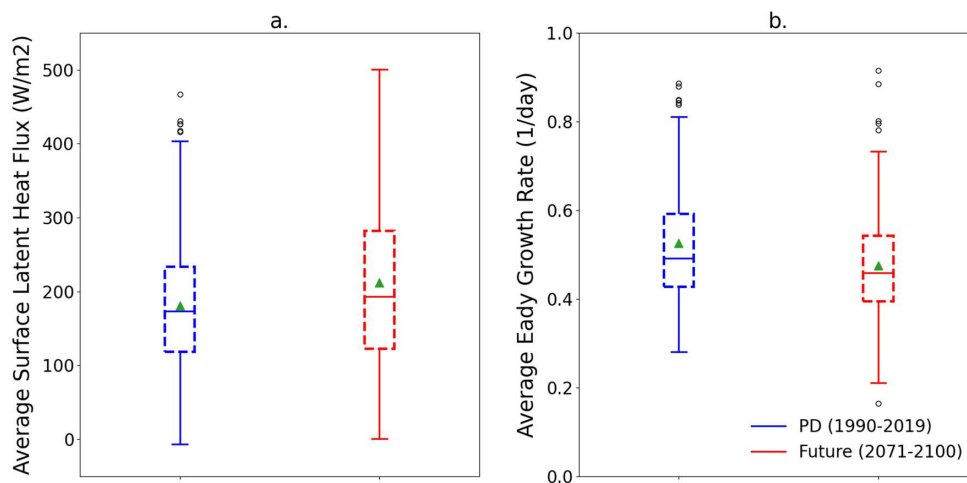
Figure 13: Box plot for the present-day experiment (blue) and the future climate simulation (red) for: a) the Surface Latent Heat Flux during, and b) the average 500-hPa Eady Growth Rate during the transition. The box represents the interquartile range (IQR) and contains 50% of the data; the upper edge of the box represents the 75th percentile (upper quartile - UQ) while the lower edge is the 25th percentile (lower quartile - LQ). The horizontal line within the box indicates the median, while the green triangle indicates the mean. The whiskers extend to the smallest and largest data points within 1.5 times the IQR from the quartiles. Points beyond the whiskers are considered outliers.

### 3.8 Reintensification during transition

Reintensification of storms during the extratropical transition (ET) phase is a critical aspect to evaluate, as it influences the overall impact and longevity of transitioning storms. Reintensification during the transition phase is assessed using pressure differences and changes in IKE. The analysis reveals that storms, on average, do not intensify during the transition, with no significant difference in the pressure change (Fig. 14 a). On average, there is a slight increase in pressure for both experiments: +3.5 hPa for the present-day simulation and +4.5 hPa for the future climate simulation. Additionally, the relative difference in IKE also shows no significant variation between the present-day and the future climate simulations (Fig. 14 b). Despite the increase in storm central pressure, there is a modest rise in IKE during the transition for both climate states (+6.6% for the present-day experiment and +7.5% for the future climate simulation), potentially driven by the increase in storm size during the transition (Kozar & Misra, 2014).
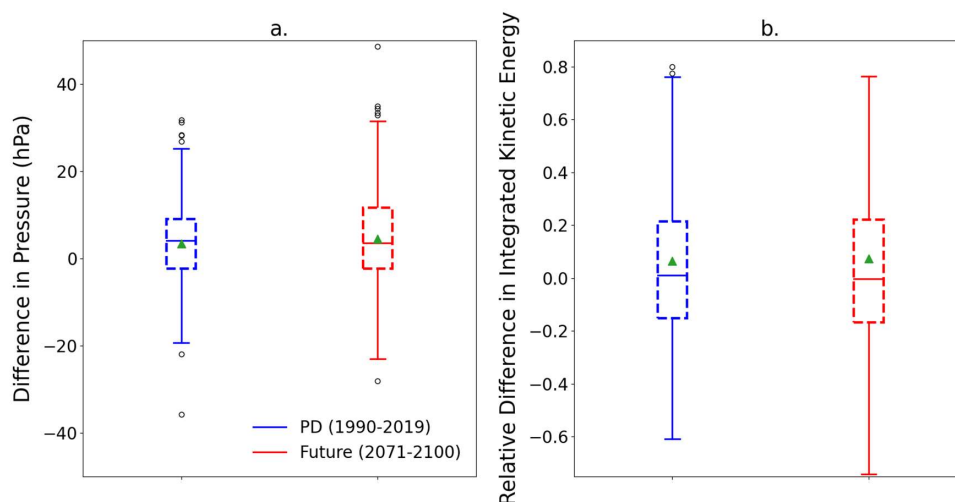
Figure 14: a) Box plot in difference in pressure at the storm center during the transition for the present-day (blue) and the future climate (red) simulations and b) Box plot in relative difference in Integrated Kinetic Energy (for present-day simulations (blue) and future climate simulations (red) during the transition. The box represents the interquartile range (IQR), containing 50% of the data; the upper edge of the box represents the 75th percentile (upper quartile - UQ) while the lower edge is the 25th percentile (lower quartile - LQ). The horizontal line within the box indicates the median, while the green triangle indicates the mean. The whiskers extend to the smallest and largest data points within 1.5 times the IQR from the quartiles. Points beyond the whiskers are considered outliers.

4. DISCUSSION AND CONCLUSIONS

This study investigates how extratropical transitions (ETs) in the North Atlantic basin might change by the end of the century under the RCP 8.5 climate scenario, using high-resolution climate simulations. While we found no significant difference in ET frequency, with the ET ratio (42.7%) in the future climate simulation being nearly identical to that in the present-day simulation (42.6%), our results indicate that transitioning storms in the future have greater potential destructiveness. Specifically, the Integrated Kinetic Energy associated with transitioning storms is significantly higher in the future climate simulation, driven largely by increased surface latent flux rather than enhanced baroclinic energy. This result aligns with the findings by Cheung and Chu (2023), which also reported an increase in the potential destructiveness of ETs.

While our findings about the ET frequency results contrast with studies by Liu et al. (2017)) and Baker et al. (2022), which reported a slight increase in ET frequency in the North Atlantic basin, our results are consistent

454 with previous research indicating that TCs will become less frequent but more intense in the future (Bender
455 et al., 2010; Knutson et al., 2020; Mallard et al., 2013). Our simulations also confirm a poleward migration
456 of the maximum intensity of TCs (Lee et al., 2020), aligning with the expansion of TC cyclogenesis regions.

457 The findings indicate that the future climate simulation show a decrease and northward shift in the mid-
458 tropospheric baroclinic zone, driven by polar amplification, along with a slight increase in the upper-
459 tropospheric baroclinic zone due to warming in the tropical upper troposphere. This weakening of the
460 baroclinic zone along with the decrease in the number of TCs explain the decrease in the number of ET
461 events, which ultimately leads to the stability of the ET frequency.

462 Additionally, our results do not show a significant change in ET seasonality, with September and October
463 remaining the primary months for ET events. However, the peak's season seems to have shifted from
464 September to October, suggesting that large-scale environmental conditions may become more favorable for
465 ET in October in the future climate simulation.

466 No significant shift in the latitude of ET onsets is simulated in the future climate simulation, although there
467 is a slight increase in ET occurrences near the U.S. Northeastern coast. This could be due to more intense
468 TCs reaching favorable baroclinic zones, which contrasts with Baker et al. (2022), who reported a decrease
469 in ET occurrences in this region, mainly explained by the poleward and eastward expansion of the
470 cyclogenesis region.

471 Previous studies (Jung & Lackmann, 2019) suggested that the duration of ETs might be longer in the future
472 due to higher SSTs, an empirical indicator of slow-transitioning storms (Hart et al., 2006), and due to reduced
473 meridional SST gradient, which inhibits baroclinic conversion. However, despite an environment that is less
474 baroclinic during ET, no significant difference in duration is simulated. However, the Cyclone Phase Space
475 methodology we use in this study has the limitation of being unable to resolve the cyclone's inner-core
476 structure (Evans et al., 2017) and hence may contribute to this finding.

477 Within the spatial zone considered, our study suggests that transitioning storms do not necessarily reintensify
478 more in a warming environment, consistent with the findings of Jung and Lackmann (2023), due to a
479 reduction in baroclinic conversion.

480 In conclusion, our study suggests that extratropical transitions will pose a greater risk for populations in the
481 U.S. Northeastern coast and the Maritimes. However, uncertainties remain regarding the impact of global
482 warming on ET frequencies and the spatial and temporal distribution of ET events. Further research is needed
483 to address these uncertainties. Future studies should investigate the large-scale environmental conditions
484 affecting the Northern Hemisphere, including East Pacific and North America. Hart and Evans (2006)
485 emphasized that storms are more likely to intensify after interacting with a negatively-tilted rather than a
486 positively-tilted trough. Therefore, a better understanding of how climate change will impact the occurrence
487 of negative-tilted versus positive-tilted troughs will be crucial for grasping future ET dynamics. Additionally,
488 the structure of post-transition storms warrants further exploration. Hart and Evans (2006) noted that warm-
489 seclusion cyclones, which are more likely to cause damage, should be examined in the context of global
490 warming. Assessing how global warming affects the post-transition structures of storms will enhance our
491 understanding of future risks associated with ETs. Hart and Evans (2001) also mentioned that 50% of tropical
492 cyclones making landfall between 1950 and 1996 were transitioning storms. Investigating the impact of
493 global warming on the spatial pattern of transitioning storms that make landfall will be important for
494 anticipating future damages. Finally, the simulations used in our study were atmospheric-only experiments
495 with prescribed SST. Baker et al. (2022) demonstrated that high-resolution fully- coupled simulations may
496 yield different outcomes compared to atmospheric-only simulations. For instance, while atmospheric-only
497 simulations showed an equatorward shift in the completion latitude, fully coupled simulations detected a
498 poleward shift. Previous studies have highlighted the necessity of considering the ocean's negative feedback
499 mechanism on tropical cyclones (Schade and Emanuel 1999; K. Emanuel et al. 2004). The winds associated
500 with tropical cyclones induce upwelling of cold waters, which cools the sea surface temperature and inhibits
501 the intensification of tropical cyclones (Schade and Emanuel 1999; K. Emanuel et al. 2004). The

502 overestimation of the maximum wind can reach up to 25 m·s⁻¹ (K. Emanuel et al. 2004). Scoccimarro et al.
503 (2017) demonstrated that a high coupling frequency could significantly reduce this bias. In the context of
504 climate change, Huang et al. (2015) showed that this ocean feedback is expected to strengthen due to the
505 increased ocean stratification, which could enhance the ocean's negative effect and reduce the expected
506 intensification of tropical cyclones in certain regions of the North Atlantic. Therefore, further investigations
507 using fully coupled models are needed to reconcile these discrepancies and build a comprehensive
508 understanding of the impacts of climate change on extratropical transitions.

509 **5. CODE AVAILABILITY**

510 The codes used are available from the corresponding author upon request.

511 **6. DATA AVAILABILITY**

512 The data used are available from the corresponding author upon request.

513 **7. AUTHOR CONTRIBUTION**

514 **Aude Garin**: Methodology, Software, Validation, Formal Analysis, Investigation, Writing - Original Draft,
515 Vizualisation. **Francesco S.R. Pausata**: Conceptualization, Methodology, Formal Analysis, Investigation,
516 Resources, Writing – Review & Editing, Vizualisation, Supervision. **Mathieu Boudreault**:
517 Conceptualization, Formal Analysis, Investigation, Resources, Writing – Review & Editing, Vizualisation,
518 Supervision. **Roberto Ingrosso**: Model Simulations, Software, Validation, Writing – Review & Editing.

519 **8. COMPETING INTERESTS**

520 The Authors declare that they have no conflict of interest.

521 **9. ACKNOWLEDGEMENTS**

522 The authors would like to thank Katja Winger for the help in developing the algorithms, Frédérik Toupin
523 and Yassine Hammadi for the technical support.

524 **10. REFERENCES**

525 Baker, A. J., Roberts, M. J., Vidale, P. L., Hodges, K. I., Seddon, J., Vannière, B., Haarsma, R. J., Schiemann,
526 R., Kapetanakis, D., Tourigny, E., Lohmann, K., Roberts, C. D., & Terray, L. (2022). Extratropical Transition
527 of Tropical Cyclones in a Multiresolution Ensemble of Atmosphere-Only and Fully Coupled Global Climate
528 Models. Journal of Climate, 35(16), 5283–5306. https://doi.org/10.1175/JCLI-D-21-0801.1

529 Bender, M. A., Knutson, T. R., Tuleya, R. E., Sirutis, J. J., Vecchi, G. A., Garner, S. T., & Held, I. M. (2010).
530 Modeled Impact of Anthropogenic Warming on the Frequency of Intense Atlantic Hurricanes. Science,
531 327(5964), 454–458. https://doi.org/10.1126/science.1180568

532 Bister, M., & Emanuel, K. A. (1998). Dissipative heating and hurricane intensity. Meteorology and
533 Atmospheric Physics, 65(3–4), 233–240. https://doi.org/10.1007/BF01030791

534 Bister, M., & Emanuel, K. A. (2002). Low frequency variability of tropical cyclone potential intensity 1.
535 Interannual to interdecadal variability. Journal of Geophysical Research: Atmospheres, 107(D24).
536 https://doi.org/10.1029/2001JD000776

537 Blender, R., Fraedrich, K., & Lunkeit, F. (1997). Identification of cyclone-track regimes in the North Atlantic.

538 Quarterly Journal of the Royal Meteorological Society, 123(539), 727–741.

539 https://doi.org/10.1002/qj.49712353910

540 Blender, R., & Schubert, M. (2000). Cyclone Tracking in Different Spatial and Temporal Resolutions.

541 Monthly Weather Review, 128(2), 377. https://doi.org/10.1175/1520-

542 0493(2000)128<0377:CTIDSA>2.0.CO;2

543 Cheung, H. M., & Chu, J.-E. (2023). Global increase in destructive potential of extratropical transition events

544 in response to greenhouse warming. Npj Climate and Atmospheric Science, 6(1), 137.

545 https://doi.org/10.1038/s41612-023-00470-8

546 Dandoy, S., Pausata, F. S. R., Camargo, S. J., Laprise, R., Winger, K., & Emanuel, K. (2021). Atlantic

547 hurricane response to Saharan greening and reduced dust emissions during the mid-Holocene. Climate of the

548 Past, 17(2), 675–701. https://doi.org/10.5194/cp-17-675-2021

549 Eady, E. T. (1949). Long Waves and Cyclone Waves. Tellus, 1(3), 33–52. https://doi.org/10.1111/j.2153-

550 3490.1949.tb01265.x

551 Emanuel, K., DesAutels, C., Holloway, C., & Korty, R. (2004). Environmental Control of Tropical Cyclone

552 Intensity. Journal of the Atmospheric Sciences, 61(7), 843–858. https://doi.org/10.1175/1520-

553 0469(2004)061<0843:ECOTCI>2.0.CO;2

554 Evans, C., & Hart, R. E. (2008). Analysis of the Wind Field Evolution Associated with the Extratropical

555 Transition of Bonnie (1998). Monthly Weather Review, 136(6), 2047–2065.

556 https://doi.org/10.1175/2007MWR2051.1

557 Evans, C., Wood, K. M., Aberson, S. D., Archambault, H. M., Milrad, S. M., Bosart, L. F., Corbosiero, K.

558 L., Davis, C. A., Dias Pinto, J. R., Doyle, J., Fogarty, C., Galarneau, T. J., Grams, C. M., Griffin, K. S.,

559 Gyakum, J., Hart, R. E., Kitabatake, N., Lentink, H. S., McTaggart-Cowan, R., … Zhang, F. (2017). The

560 Extratropical Transition of Tropical Cyclones. Part I: Cyclone Evolution and Direct Impacts. Monthly

561 Weather Review, 145(11), 4317–4344. https://doi.org/10.1175/MWR-D-17-0027.1

562 Garner, A. J., Kopp, R. E., & Horton, B. P. (2021). Evolving Tropical Cyclone Tracks in the North Atlantic

563 in a Warming Climate. Earth's Future, 9(12), e2021EF002326. https://doi.org/10.1029/2021EF002326

564 Gilford, D. M. (2021). pyPI (v1.3): Tropical Cyclone Potential Intensity Calculations in Python.

565 Geoscientific Model Development, 14(5), 2351–2369. https://doi.org/10.5194/gmd-14-2351-2021

566 Gualdi, S., Scoccimarro, E., & Navarra, A. (2008). Changes in Tropical Cyclone Activity due to Global

567 Warming: Results from a High-Resolution Coupled General Circulation Model. Journal of Climate, 21(20),

568 5204–5228. https://doi.org/10.1175/2008JCLI1921.1

569 Harr, P. A., & Elsberry, R. L. (2000). Extratropical Transition of Tropical Cyclones over the Western North

570 Pacific. Part I: Evolution of Structural Characteristics during the Transition Process. Monthly Weather

571 Review, 128(8), 2613–2633. https://doi.org/10.1175/1520-0493(2000)128<2613:ETOTCO>2.0.CO;2

572 Hart, R. E. (2003). A Cyclone Phase Space Derived from Thermal Wind and Thermal Asymmetry. Monthly

573 Weather Review, 131(4), 585–616. https://doi.org/10.1175/1520-0493(2003)131<0585:ACPSDF>2.0.CO;2

574   Hart, R. E., & Evans, J. L. (2001). A Climatology of the Extratropical Transition of Atlantic Tropical

575   Cyclones. Journal of Climate, 14(4), 546–564. https://doi.org/10.1175/1520-

576   0442(2001)014<0546:ACOTET>2.0.CO;2

577   Hart, R. E., Evans, J. L., & Evans, C. (2006). Synoptic Composites of the Extratropical Transition Life Cycle

578   of North Atlantic Tropical Cyclones: Factors Determining Posttransition Evolution. Monthly Weather

579   Review, 134(2), 553–578. https://doi.org/10.1175/MWR3082.1

580   Hersbach, H., Bell, B., Berrisford, P., Hirahara, S., Horányi, A., Muñoz-Sabater, J., Nicolas, J., Peubey, C.,

581   Radu, R., Schepers, D., Simmons, A., Soci, C., Abdalla, S., Abellan, X., Balsamo, G., Bechtold, P., Biavati,

582   G., Bidlot, J., Bonavita, M., … Thépaut, J. (2020). The ERA5 global reanalysis. Quarterly Journal of the

583   Royal Meteorological Society, 146(730), 1999–2049. https://doi.org/10.1002/qj.3803

584   Hill, K. A., & Lackmann, G. M. (2011). The Impact of Future Climate Change on TC Intensity and Structure:

585   A Downscaling Approach. Journal of Climate, 24(17), 4644–4661. https://doi.org/10.1175/2011JCLI3761.1

586   Huang, P., Lin, I.-I., Chou, C., & Huang, R.-H. (2015). Change in ocean subsurface environment to suppress

587   tropical cyclone intensification under global warming. Nature Communications, 6(1), 7188.

588   https://doi.org/10.1038/ncomms8188

589   Ingrosso, R., & Pausata, F. S. R. (2024). Contrasting consequences of the Great Green Wall: Easing aridity

590   while increasing heat extremes. One Earth, 7(3), 455–472. https://doi.org/10.1016/j.oneear.2024.01.017

591   Jones, S. C., Harr, P. A., Abraham, J., Bosart, L. F., Bowyer, P. J., Evans, J. L., Hanley, D. E., Hanstrum, B.

592   N., Hart, R. E., Lalaurette, F., Sinclair, M. R., Smith, R. K., & Thorncroft, C. (2003). The Extratropical

593   Transition of Tropical Cyclones: Forecast Challenges, Current Understanding, and Future Directions.

594   Weather and Forecasting, 18(6), 1052–1092. https://doi.org/10.1175/1520-

595   0434(2003)018<1052:TETOTC>2.0.CO;2

596   Jung, C., & Lackmann, G. M. (2019). Extratropical Transition of Hurricane Irene (2011) in a Changing

597   Climate. Journal of Climate, 32(15), 4847–4871. https://doi.org/10.1175/JCLI-D-18-0558.1

598   Jung, C., & Lackmann, G. M. (2021). The Response of Extratropical Transition of Tropical Cyclones to

599   Climate Change: Quasi-Idealized Numerical Experiments. Journal of Climate, 34(11), 4361–4381.

600   https://doi.org/10.1175/JCLI-D-20-0543.1

601   Jung, C., & Lackmann, G. M. (2023). Changes in Tropical Cyclones Undergoing Extratropical Transition in

602   a Warming Climate: Quasi-Idealized Numerical Experiments of North Atlantic Landfalling Events.

603   Geophysical Research Letters, 50(8), e2022GL101963. https://doi.org/10.1029/2022GL101963

604   Klein, P. M., Harr, P. A., & Elsberry, R. L. (2000). Extratropical Transition of Western North Pacific Tropical

605   Cyclones: An Overview and Conceptual Model of the Transformation Stage. Weather and Forecasting, 15(4),

606   373–395. https://doi.org/10.1175/1520-0434(2000)015<0373:ETOWNP>2.0.CO;2

607   Knapp, K. R., Kruk, M. C., Levinson, D. H., Diamond, H. J., & Neumann, C. J. (2010). The International

608   Best Track Archive for Climate Stewardship (IBTrACS): Unifying Tropical Cyclone Data. Bulletin of the

609   American Meteorological Society, 91(3), 363–376. https://doi.org/10.1175/2009BAMS2755.1

610   Knutson, T., Camargo, S. J., Chan, J. C. L., Emanuel, K., Ho, C.-H., Kossin, J., Mohapatra, M., Satoh, M.,
611   Sugi, M., Walsh, K., & Wu, L. (2020). Tropical Cyclones and Climate Change Assessment: Part II: Projected
612   Response to Anthropogenic Warming. Bulletin of the American Meteorological Society, 101(3), E303–E322.
613   https://doi.org/10.1175/BAMS-D-18-0194.1

614   Kossin, J. P., Emanuel, K. A., & Vecchi, G. A. (2014). The poleward migration of the location of tropical
615   cyclone maximum intensity. Nature, 509(7500), 349–352. https://doi.org/10.1038/nature13278

616   Kossin, J. P., Knapp, K. R., Olander, T. L., & Velden, C. S. (2020). Global increase in major tropical cyclone
617   exceedance probability over the past four decades. Proceedings of the National Academy of Sciences,
618   117(22), 11975–11980. https://doi.org/10.1073/pnas.1920849117

619   Kozar, M. E., & Misra, V. (2014). Statistical Prediction of Integrated Kinetic Energy in North Atlantic
620   Tropical Cyclones. Monthly Weather Review, 142(12), 4646–4657. https://doi.org/10.1175/MWR-D-14-
621   00117.1

622   Lee, C.-Y., Camargo, S. J., Sobel, A. H., & Tippett, M. K. (2020). Statistical–Dynamical Downscaling
623   Projections of Tropical Cyclone Activity in a Warming Climate: Two Diverging Genesis Scenarios. Journal
624   of Climate, 33(11), 4815–4834. https://doi.org/10.1175/JCLI-D-19-0452.1

625   Lehmann, J., Coumou, D., Frieler, K., Eliseev, A. V., & Levermann, A. (2014). Future changes in
626   extratropical storm tracks and baroclinicity under climate change. Environmental Research Letters, 9(8),
627   084002. https://doi.org/10.1088/1748-9326/9/8/084002

628   Lindzen, R. S., & Farrell, B. (1980). A Simple Approximate Result for the Maximum Growth Rate of
629   Baroclinic   Instabilities.   Journal   of   the   Atmospheric   Sciences,   37(7),   1648–1654.
630   https://doi.org/10.1175/1520-0469(1980)037<1648:ASARFT>2.0.CO;2

631   Liu, M., Vecchi, G. A., Smith, J. A., & Murakami, H. (2017). The Present-Day Simulation and Twenty-First-
632   Century Projection of the Climatology of Extratropical Transition in the North Atlantic. Journal of Climate,
633   30(8), 2739–2756. https://doi.org/10.1175/JCLI-D-16-0352.1

634   Mallard, M. S., Lackmann, G. M., & Aiyyer, A. (2013). Atlantic Hurricanes and Climate Change. Part II:
635   Role of Thermodynamic Changes in Decreased Hurricane Frequency. Journal of Climate, 26(21), 8513–
636   8528. https://doi.org/10.1175/JCLI-D-12-00183.1

637   Michaelis, A. C., & Lackmann, G. M. (2019). Climatological Changes in the Extratropical Transition of
638   Tropical Cyclones in High-Resolution Global Simulations. Journal of Climate, 32(24), 8733–8753.
639   https://doi.org/10.1175/JCLI-D-19-0259.1

640   Michaelis, A. C., & Lackmann, G. M. (2021). Storm-Scale Dynamical Changes of Extratropical Transition
641   Events in Present-Day and Future High-Resolution Global Simulations. Journal of Climate, 34(12), 5037–
642   5062. https://doi.org/10.1175/JCLI-D-20-0472.1

643   Powell, M. D., & Reinhold, T. A. (2007). Tropical Cyclone Destructive Potential by Integrated Kinetic
644   Energy. Bulletin of the American Meteorological Society, 88(4), 513–526. https://doi.org/10.1175/BAMS-
645   88-4-513

646   Rantanen, M., Räisänen, J., Sinclair, V. A., & Lento, J. (2020). The extratropical transition of Hurricane
647   Ophelia (2017) as diagnosed with a generalized omega equation and vorticity equation. Tellus A: Dynamic
648   Meteorology and Oceanography, 72(1), 1721215. https://doi.org/10.1080/16000870.2020.1721215
649   Schade, L. R., & Emanuel, K. A. (1999). The Ocean's Effect on the Intensity of Tropical Cyclones: Results
650   from a Simple Coupled Atmosphere–Ocean Model. Journal of the Atmospheric Sciences, 56(4), 642–651.
651   https://doi.org/10.1175/1520-0469(1999)056<0642:TOSEOT>2.0.CO;2
652   Schubert, M., Perlwitz, J., Blender, R., Fraedrich, K., & Lunkeit, F. (1998). North Atlantic cyclones in CO 2
653   -induced warm climate simulations: Frequency, intensity, and tracks. Climate Dynamics, 14(11), 827–838.
654   https://doi.org/10.1007/s003820050258
655   Scoccimarro, E., Fogli, P. G., Reed, K. A., Gualdi, S., Masina, S., & Navarra, A. (2017). Tropical Cyclone
656   Interaction with the Ocean: The Role of High-Frequency (Subdaily) Coupled Processes. Journal of Climate,
657   30(1), 145–162. https://doi.org/10.1175/JCLI-D-16-0292.1
658   Studholme, J., Fedorov, A. V., Gulev, S. K., Emanuel, K., & Hodges, K. (2022). Poleward expansion of
659   tropical   cyclone   latitudes   in   warming   climates.   Nature   Geoscience,   15(1),   14–28.
660   https://doi.org/10.1038/s41561-021-00859-1
661   Zarzycki, C. M., Thatcher, D. R., & Jablonowski, C. (2017). Objective tropical cyclone extratropical
662   transition detection in high-resolution reanalysis and climate model data. Journal of Advances in Modeling
663   Earth Systems, 9(1), 130–148. https://doi.org/10.1002/2016MS000775
664